Inorganic Chemistry

Article

pubs.acs.org/IC

Mechanism of "Turn-on" Fluorescent Sensors for Mercury(II) in Solution and Its Implications for Ligand Design

Hyunjung Lee,[†] Hee-Seung Lee,[†] Joseph H. Reibenspies,[‡] and Robert D. Hancock*[,†]

[†]Department of Chemistry and Biochemistry, University of North Carolina, Wilmington, Wilmington, North Carolina 28403, United States

[‡]Department of Chemistry, Texas A&M University, College Station, Texas 77843, United States

ABSTRACT: The tendency of a Hg^{II} ion to strongly quench fluorescence of potential fluorescent sensors is explored. Fluorescence measurements show the expected order of the chelation-enhanced fluorescence (CHEF) effect of $Zn^{II} > Cd^{II} \gg Hg^{II} \sim Cu^{II}$, which is interpreted as (1) unpaired electrons causing the weak CHEF effect for Cu^{II} and (2) the order $Zn^{II} > Cd^{II} \gg Hg^{II}$ reflecting the "heavy atom" effect, which may be due to increasing spin−orbit coupling constants (ζ) for $Zn^{II} < Cd^{II} \ll Hg^{II}$. The structures of mercury(II) complexes of *N*-(9-anthracenylmethyl)-*N*-(2-pyridinylmethyl)-2-pyridinemethanamine (ADPA) are reported. $[Hg(ADPA)Cl_2HgCl_2]$ (**1**) has one Hg^{II} held by two bridging chlorides, while the other Hg^{II} is coordinated to the ADPA ligand. The latter Hg^{II} has a nearest π contact of 3.215 Å with a C atom from the anthracenyl group, which falls in the range of reported Hg−C π contacts with aromatic groups. This contact may be important in quenching the fluorescence of the Hg^{II}/ADPA complex. A density functional theory study shows that the Hg−C interaction is strong enough to prevent a simple HOMO → LUMO transition of the fluorophore. In fact, the $S_0 \rightarrow S_1$ and S_2 transitions in the Hg^{II}/ADPA complex have significant charge-transfer character to mercury. An important aspect of the coordination geometry of Hg^{II} is illustrated by **1**, where Hg^{II} tends to form a few (often only two) short bonds to the more covalently binding donor atoms present, with much longer bonds to other donor atoms. The Hg−N bonds to the two pyridyl N-donor atoms of ADPA in **1** are relatively short at 2.212(8) and 2.224(8) Å, while that to the central saturated N-donor atom of ADPA is long at 2.603(8) Å. The latter long Hg−N bond may allow a photoinduced electron-transfer (PET) effect, quenching the fluorescence of the anthracenyl fluorophore. The structure of $[Hg(ADPA)Br_2]$ (**2**) reflects the more covalent binding of the two bromine ligands compared to the clorine ligands of **1**, with much longer Hg−C contacts with the anthracenyl fluorophore and a Hg−N contact with the saturated N atom of ADPA of 2.917 Å. The latter long Hg−N contact is related to the nearly negligible fluorescence of the ADPA complex in the presence of added Br^-. The addition of extra ligands to the Hg^{II}/ADPA complex produces a weak increase in the fluorescence intensity for $OH^- \sim Cl^- \gg Br^- > I^-$, which is discussed in terms of an increasing PET effect, and to collisional quenching. The ligand design principles for generating turn-on sensors for mercury suggested by this work are discussed.

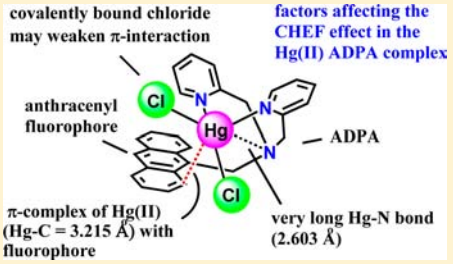

INTRODUCTION

The development of fluorescent sensors for Hg^{II} is of considerable interest because of the extreme toxicity of mercury.[1−3] Fluorescent sensors that show an increase in the fluorescence intensity in the presence of a coordinated metal ion function by the chelation-enhanced fluorescence (CHEF) effect.[4−10] Briefly, such sensors have a lone pair of suitable energy, which can quench the fluorescence by virtue of the photoinduced electron-transfer (PET) effect. In the PET effect, the quenching orbital (e.g., the lone pair on an adjacent amine group) is of higher energy than the highest occupied molecular orbital (HOMO) of the fluorophore (e.g., an extended aromatic group). Upon excitation of an electron from the HOMO to an excited state of the fluorophore, an electron drops from the lone pair into the gap in the HOMO of the fluorophore and prevents the excited electron from falling back to the ground state, quenching the fluorescence. In the CHEF effect, a metal ion coordinates to the quenching lone pair and drops the energy of the lone pair below that of the ground state of the fluorophore, so that fluorescence is restored. This is summarized in Scheme 1.

Scheme 1. In the Excited State of the Fluorophore: (a) Fluorescence Quenched by the PET Effect and (b) Fluorescence Restored by the CHEF Effect

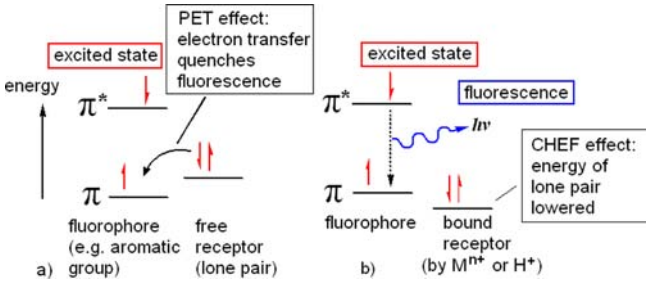

Received: June 27, 2012
Published: September 24, 2012

Metal ions that are particularly good at producing a CHEF effect are[11,12] Ca^{II} and Zn^{II} and to a lesser extent Cd^{II}. Many other metal ions do not usually produce a CHEF effect, and this includes Hg^{II}, which is usually good at quenching the fluorescence,[13] producing a negative or "turn-off" chelation-enhanced quenching (CHEQ) effect. Three properties of metal ions that appear[14] to affect the production of a CHEF effect are as follows: (1) Heavy metal ions such as Hg^{II} and Pb^{II} are of high Z (atomic weight) and thus have large spin−orbit coupling constants (ζ).[15,16] It is believed that large ζ values stabilize the triplet state, leading to longer lifetimes in the excited state and thus a greater tendency to return to the ground state by radiationless relaxation. (2) Paramagnetic d-block metal ions such as Cu^{II} or high-spin Ni^{II}, as well as paramagnetic f-block metal ions such as Gd^{III} or Tm^{III}, strongly quench fluorescence. (3) Metal ions such as Ca^{II} and Zn^{II}, have a relatively low value of Z, are not paramagnetic, and are able to coordinate fully to all of the potentially quenching lone pairs of the ligand, producing a strong CHEF effect. (4) A further factor is[17−20] the fact that if M−L bonds, where L is the donor atom containing the quenching lone pair, are distorted by steric effects, overlap with the quenching lone pair will be diminished, and the CHEF effect may be weakened or not be manifested at all.

One distinguishes between fluorescent sensors where the fluorophore contains heteroatoms (typically, N-donor atoms such as are present in PDA or DPP,[21] which bind directly to the metal ion being sensed) and fluorophores that are separated from the ligand that binds the metal ion by a linker and contain no heteroatoms, such as the anthracenyl group of *N*-(9-anthracenylmethyl)-*N*-(2-pyridinylmethyl)-2-pyridinemethanamine (ADPA) studied in this work. One might refer to these respectively as coordinated and tethered fluorophores. Examples of coordinated[19] and tethered[22] fluorophores are shown in Scheme 2.

Scheme 2. Examples of (a) Coordinated and (b) Tethered Fluorophores in Metal-Ion Fluorescent Sensors

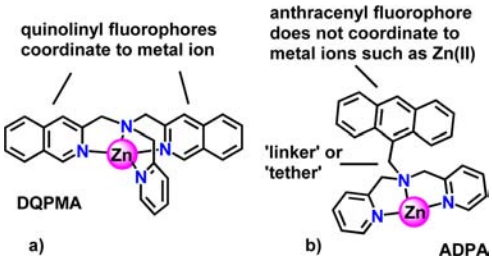

The most desirable fluorescent sensors for metal ions are "turn-on" sensors that display a positive CHEF effect rather than a CHEQ effect.[22] The majority of sensors reported for Hg^{II} are "turn-off" sensors[13,22] because Hg^{II} produces mostly a CHEQ effect, presumably because of the high ζ value. It appears, however, that, for large ζ values to quench fluorescence, covalent bonding to donor atoms that are part of the fluorophore may be necessary.[23] In fact, although diamagnetic metal ions such as La^{III} or Lu^{III} have large ζ values, they cause large "turn-on" CHEF effects with ligands such as PDA (see Figure 1 for the key to ligand abbreviations) presumably because the bonding to the N-donor atoms that are part of the fluorophore is very ionic. (By ionic here is meant, of course, that the donor atoms of the ligand largely retain the negative charge present in the donor orbitals, and the M−L bond is stabilized largely by an electrostatic attraction between this negative charge and the positive charge on the metal cation. This is in contrast to covalent bonding, where the charge is more evenly shared between the two atoms forming the bond.) It is not entirely clear whether the CHEQ effect produced by the ions with high Z values is due to large spin−orbit coupling effects, covalent interaction with the fluorophores, or a combination of both.

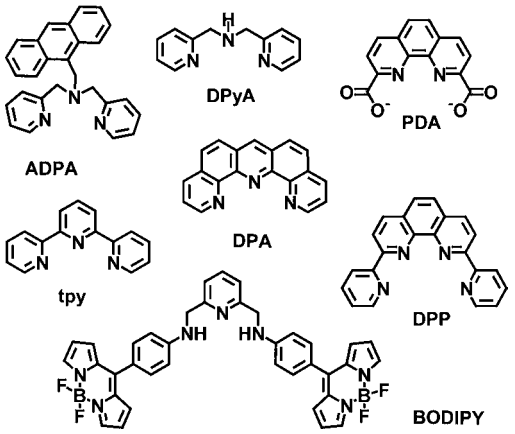

Figure 1. Some ligands discussed in this paper.

In this paper, the fact that Hg^{2+} in solution strongly quenches the fluorescence of ADPA is investigated crystallographically for some mercury(II) complexes of ADPA, supported by density functional theory (DFT) calculations. The point of interest is how Hg^{II} quenches the fluorescence of ADPA if such quenching requires covalent bonding to the fluorophore. Czarnik et al.[22] suggested that quenching of the fluorescence in **L1** was possible because Hg^{II} could form a π complex with the anthracenyl group present. This suggestion is illustrated in Scheme 3, with a somewhat modified structure suggested for the complex based on molecular modeling by the present authors using *HyperChem*.[25]

Scheme 3. Possible Structure of a Mercury(II) Complex of L1 That Leads to Quenching of the Fluorescence via Formation of a π Complex between Hg^{II} and the Anthracenyl Fluorophore of L1[22]

The structure of the copper(II) complex of ADPA is also investigated as an example where the anthracenyl group of ADPA is not coordinated to the metal ion. In addition, the effect of the addition of halide ions on the fluorescence of the mercury(II) complex of ADPA is investigated. It appeared possible that coordination of further ligands such as halide ions or hydroxide to the Hg^{II}/ADPA complex might displace the coordinated anthracenyl group from Hg^{II} and so restore its fluorescence, leading to a novel type of anion sensor.

dx.doi.org/10.1021/ic301380w | *Inorg. Chem.* 2012, 51, 10904−10915

EXPERIMENTAL SECTION

Materials. ADPA was synthesized following a literature method.[26] The metal salts $HgCl_2$, $HgBr_2$, and $Cu(NO_3)_2$ and metal perchlorates were obtained from VWR or Strem in ≥99% purity and used as received. All solutions were prepared in deionized water (Milli-Q, Waters Corp.) of >18 MΩ·cm^{-1} resistivity, plus high-performance liquid chromatography (HPLC)-grade methanol (MeOH) from Merck.

Synthesis of Mercury(II) Complexes of ADPA. The general procedure followed for the synthesis of mercury(II) complexes with ADPA was as follows: 1 equiv of ADPA (58.4 mg, 0.15 mmol) was dissolved in acetonitrile (3 mL) and added to a solution of 1 equiv of the metal salt ($HgCl_2$ or $HgBr_2$) in acetonitrile (1 mL). A total of 2 mL of toluene was added to this solution, and the resulting solution was set aside for slow evaporation of the solvent in the refrigerator. Yellow crystals precipitated in several days. The solutions were filtered under vacuum, and the solids were air-dried.

$[Hg(ADPA)Cl_2HgCl_2]$ (**1**): yellow crystals. Repeated elemental analyses on samples combining several crystals suggested that some $[Hg(ADPA)Cl_2]$ was also present in the sample. The C and N elemental compositions of some individual crystals were measured with a CE Elantech model NC 2100CHN analyzer.[27] This confirmed that the more numerous small crystals present were **1**, with C and N analyses (average of three crystals) as follows. Calcd for $C_{27}H_{23}Cl_4Hg_2N_3$: C, 34.78; N, 4.51. Found: C, 34.81; N, 4.42. Two large crystals gave average analyses in agreement with the presence of the $[Hg(ADPA)Cl_2]$ complex. Calcd for $C_{27}H_{23}Cl_2HgN_3$: C, 49.06; N, 6.36. Found: C, 48.67; N, 6.36. Some powder at the bottom of the sample vial gave an analysis of C, 38.49, and N, 4.91, in agreement with the presence of a sample containing predominantly **1**. A powder X-ray diffraction pattern of the bulk sample matched the theoretical diffraction pattern for **1** generated using the *Mercury* program.[28] A small crystal of the type that gave an elemental analysis corresponding to **1** was selected for structural analysis.

$[Hg(ADPA)Br_2]$ (**2**): yellow crystals. Elem anal. Calcd for $C_{27}H_{23}Br_2HgN_3$: C, 43.24; H, 3.09; N 5.60. Found: C, 43.36; H, 3.02; N, 5.95.

Synthesis of Copper(II) Complexes of ADPA. A total of 1 equiv of ADPA (35 mg, 0.09 mmol) was dissolved in MeOH (4 mL) and added to a solution of 1 equiv of $Cu(NO_3)_2$ in MeOH (3 mL). Diffusion of diethyl ether vapor into this solution resulted in dark-green crystals. The solutions were filtered under vacuum, and the crystals were air-dried. $[Cu(ADPA)(NO_3)_2]$ (**3**): green crystals. Elem anal. Calcd for $C_{27}H_{23}CuN_5O_6$: C, 56.00; H, 4.00; N, 12.09. Found: C, 56.39; H, 3.92; N, 12.39.

Molecular Structure Determination. A Bruker D8-GADDS X-ray (three-circle) diffractometer was employed for crystal screening, unit cell determination, and data collection. The structures were solved by direct methods and refined to convergence.[29] Some details of the structure determination are given in Table 1, and crystal coordinates and details of the structure determination of **1**–**3** have been deposited with the CSD (Cambridge Structural Database).[28] A selection of bond lengths and angles for **1**–**3** are given in Tables 3–5. The structures of **1**–**3** are shown in Figures 8, 9, and 11.

Fluorescence Measurements. Excitation–emission matrix (EEM) fluorescence properties were determined on a Jobin Yvon SPEX Fluoromax-3 scanning fluorometer equipped with a 150 W xenon arc lamp and a R928P detector. The instrument was configured to collect the signal in ratio mode with dark offset using 5 nm bandpasses on both the excitation and emission monochromators. The EEMs were created by concatenating emission spectra measured every 5 nm from 250 to 500 nm at 51 separate excitation wavelengths. Scans were corrected for instrument configuration using factory-supplied correction factors. The postprocessing of scans was performed using the *FluorEssence* program.[30] The software eliminates Rayleigh and Raman scattering peaks by excising portions (±10–15 nm FW) of each scan centered on the respective scatter peak. The excised data are replaced using three-dimensional interpolation of the remaining data according to the Delaunay triangulation method and constraining the interpolation such that all nonexcised data are retained. Following the removal of scatter peaks, data were normalized to a daily determined water Raman intensity (275ex/303em, 5 nm bandpasses). Replicate scans were generally within 5% agreement in terms of intensity and within bandpass resolution in terms of peak location. The fluorescence of the ADPA solutions was recorded in 50% MeOH/water.

Table 1. Crystal Data and Details of Structure Refinement for 1–3

	1	2	3
empirical formula	$C_{27}H_{23}Cl_4Hg_2N_3$	$C_{27}H_{23}Br_2HgN_3$	$C_{27}H_{23}CuN_5O_6$
fw	932.46	749.89	577.04
temperature (K)	110(2)	110(2)	110(2)
wavelength (Å)	0.71073	0.71073	0.71073
cryst syst	monoclinic	monoclinic	triclinic
space group	$P2_1/c$	$P2_1/c$	$P\bar{1}$
unit cell dimens			
a (Å)	9.115(8)	15.2870(7)	9.5519(4)
b (Å)	15.125(15)	7.7255(3)	14.1153(6)
c (Å)	19.789(19)	21.8265(11)	19.4626(11)
α (deg)	90	90	69.114(3)
β (deg)	98.818(15)	110.401(2)	88.688(3)
γ (deg)	90	90	76.206(2)
volume (Å^3)	2696(4)	2414.60(19)	2375.4(2)
Z	4	4	4
final R indices [$I > 2\sigma(I)$]	R1 = 0.0510, wR2 = 0.1100	R1 = 0.0337, wR2 = 0.0722	R1 = 0.0318, wR2 = 0.0878
R indices (all data)	R1 = 0.0667, wR2 = 0.1181	R1 = 0.0485, wR2 = 0.0775	R1 = 0.0372, wR2 = 0.0901

DFT Calculations. All DFT/time-dependent DFT (TDDFT) calculations reported in this work were carried out with the *ab initio* quantum chemistry package *GAMESS*.[31] Geometry optimization of the Hg^{II}/ADPA complexes was performed within the framework of Kohn–Sham DFT with a B3LYP exchange-correlation functional.[32,33] The SV(P) basis set[34] was used for the main-group elements, whereas the Lanl2DZ[35–37] effective core potential was employed for mercury. All DFT/TDDFT calculations were performed in an aqueous solution environment using a polarizable continuum model (PCM) as implemented in *GAMESS*.

Equilbrium Constant Determinations. The protonation constants for ADPA in 50% MeOH were determined from fluorescence spectra as a function of the pH. Variation of the fluorescence intensity as a function of the pH at five different wavelengths was fitted using the *Solver* module of the *EXCEL* program to yield two protonation constants.[38] A VWR sympHony SR60IC pH meter with a VWR sympHony gel epoxy semimicro combination pH electrode was used for all pH readings, which were made in the external titration cell, with N_2 bubbled through the cell to exclude CO_2. Aliquots were transferred from the external titration cell to the fluorometer using a Pasteur pipet in order to record the spectra.

The metal-ion formation constants for Zn^{II} and Cd^{II} (Figure 3) were determined by monitoring the fluorescence intensity of 5×10^{-6} M ADPA at pH 6.4 in 50% MeOH at five wavelengths as a function of the metal-ion concentration. ADPA (pK_a = 7.14) was present at pH 6.4 largely as the monoprotonated free ligand, which was corrected for in calculating log K_1. Variation in the fluorescence intensity as a function of the metal-ion concentration was fitted to yield the values of log K_1 reported in Table 2 using the *Solver* module available as part of the *EXCEL* program.[38] Determination of the log K_1 value for Hg^{II} with ADPA proved more challenging because the complex was too stable for log K_1 to be determined by the method employed for Zn^{II} and Cd^{II}. The complex was also too stable to be studied by the method of competition with the proton because the complex was not broken up at even the lowest pH values. It was found that the complex could be broken up at higher pH by displacement of ADPA by OH^- to give the solution species $Hg(OH)_2$. No value of log β_2 for Hg^{2+} with OH^- has

dx.doi.org/10.1021/ic301380w | Inorg. Chem. 2012, 51, 10904–10915

Table 2. Protonation and Formation Constants of ADPA (L) in 50% MeOH/Water at 25 °C, As Determined by Fluorescence Measurements[a]

equilibrium	log K of ADPA (50% MeOH)[b]	log K of DPyA (water)[c]
$L + H^+ \leftrightarrows LH^+$	7.14(3)	7.20
$LH^+ + H^+ \leftrightarrows LH_2^{2+}$	4.70(3)[d]	2.50
$Zn^{2+} + L \leftrightarrows ZnL^{2+}$	6.41(5)	7.63
$Cd^{2+} + L \leftrightarrows CdL^{2+}$	5.48(5)	6.4
$HgL^{2+} + 2OH^- \leftrightarrows Hg(OH)_2(aq) + L$	5.2(1)	(4)[e]
$HgL^{2+} + OH^- \leftrightarrows HgLOH^+$	6.3(1)	6.3[f]
$Hg^{2+} + L \leftrightarrows HgL^{2+}$	(16)[g]	(17)[e]

[a]The corresponding constants for the similar DPyA ligand reported in water are given for comparison.[37]. [b]This work at μ = 0 and 25 °C. [c]From reference 37. [d]As discussed in the text, this high pK value may refer to protonation of an excited state. [e]log K_1 for DPyA with Hg^{II} estimated from the known log β_2 = 22.25 for Hg^{II} with DPyA,[37] compared to log K_1 = 21.8 and log β_2 = 29.0 for dien with Hg^{II}.[37] [f]This refers to hydrolysis of the Hg^{II}/dien complex. [g]Log β_2 is not known for Hg^{2+} and OH^- in 50% MeOH, so that this constant was calculated using log β_2 = 21.2 for Hg^{2+} and OH^- in water and so is only approximate.[37]

been reported in 50% MeOH, and this value is necessary to obtain log K_1 for Hg^{II} with ADPA from the competition reaction between ADPA and OH^- studied here. In Table 2 is thus reported the equilibrium constant first for the formation of $[Hg(ADPA)OH]^+$ as the pH is raised and then for the displacement of ADPA to give $Hg(OH)_2(aq)$ and free ADPA ligand. An approximate value of K_1 for Hg^{II} with ADPA is obtained by combing the reported[39] log β_2 for Hg^{II} with OH^- in aqueous solution with the constants for displacement of ADPA by OH^- in 50% MeOH.

That the log K values determined here for ADPA with Zn^{II}, Cd^{II}, and Hg^{II} are reasonable is shown in Table 2 by comparing them with the log K values determined in aqueous solution for the similar DPyA ligand.[39] It should be borne in mind, as discussed below, that protonation and formation constants determined by fluorescence measurements may be inaccurate because the fluorescence being monitored relates to excited-state species rather than ground-state species of interest in the usual formation constants.

RESULTS AND DISCUSSION

Fluorescence and Thermodynamic Stability of ADPA Complexes. The fluorescence spectra of the 2 × 10^{-6} M ADPA complexes of Zn^{II}, Cd^{II}, Hg^{II}, and Cu^{II} in 50% MeOH are shown in Figure 2. As mentioned in the Introduction, the CHEF effects produced by the metal ions follow the usual order expected from the effect of increasing values of Z and ζ of $Zn^{II} > Cd^{II} \gg Hg^{II}$.[14] The presence of an unpaired electron in the copper(II) complex accounts for its very low fluorescence intensity.[14] Czarnik et al. suggested that, in a complex of mercury(II) with the ADPA type of ligand, fluorescence was quenched because of the formation of a π complex between Hg^{II} and the anthracenyl fluorophore,[22] the interaction of which is believed to be necessary to communicate the quenching effects of a large ζ from Hg^{II} to the fluorophore.

In Figure 3 is shown variation of the intensity of emission of 5 × 10^{-6} M ADPA in 50% MeOH as a function of the Cd^{2+} concentration at pH 6.4. Variation of the emission intensity at five different wavelengths as a function of the Cd^{2+} concentration was fitted using *EXCEL*[38] to yield the log K_1 value for Cd^{II} with ADPA given in Table 2. The spectra are recorded without a background electrolyte to control the ionic strength because added electrolytes have been found to salt out

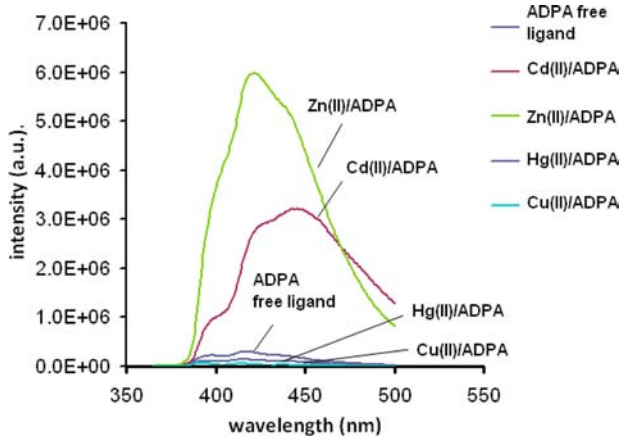

Figure 2. Fluorescence spectra of 10^{-6} M ADPA solutions (50% MeOH/H_2O), as well as of the complexes of ADPA with Zn^{II}, Cd^{II}, Hg^{II}, and Cu^{II}, and also 10^{-6} M in 50% MeOH/H_2O. Wavelength of excitation = 350 nm.

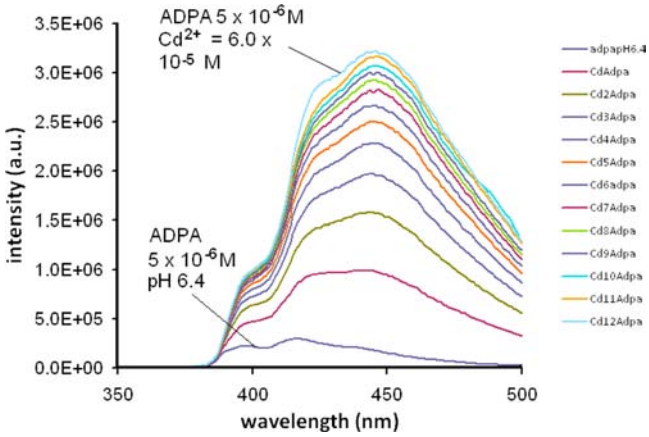

Figure 3. Fluorescence of 5 × 10^{-6} M ADPA in 50% MeOH/water as a function of the $[Cd^{2+}]$ concentration at pH 6.4 and 25 °C. The lowest spectrum has no added Cd^{2+}, and the Cd/ADPA ratios increase monotonically from 1:1, 2:1, up to 12:1 (topmost spectrum). Wavelength of excitation = 350 nm.

ligands of low solubility such as tpy and DPA.[40,41] ADPA (pK_a = 7.14) was present at pH 6.4 largely as the monoprotonated free ligand, which was corrected for in the calculation of log K_1. log K_1 was also determined for the Zn^{II}/ADPA complex in 50% MeOH in a manner analogous to that for Cd^{II}. Hg^{II} presents a challenge in determining log K_1 because its formation constants, particularly with N-donor ligands, can be extremely large.[39] This means the failure of some methods for determining log K_1, such as monitoring the competition between the metal ion and proton for binding to the ligand at lower pH values because the complex is not broken up even at the lowest pH values. One possibility is to monitor the fluorescence of the Hg^{II}/ADPA complex as a function of the higher pH, so that log K_1 might be calculated from equilibrium (1).

$$Hg(ADPA)^{2+} + 2OH^- \rightleftarrows Hg(OH)_2(aq) + ADPA \quad (1)$$

In Figure 4 are shown the fluorescence spectra at a variety of pH values of 1:1 Hg^{II}/ADPA solutions at 5 × 10^{-6} M in 50% MeOH. For purposes of comparison and also for calculation of the pK_a values of ADPA, the spectra of 5 × 10^{-6} M ADPA in

dx.doi.org/10.1021/ic301380w | Inorg. Chem. 2012, 51, 10904−10915

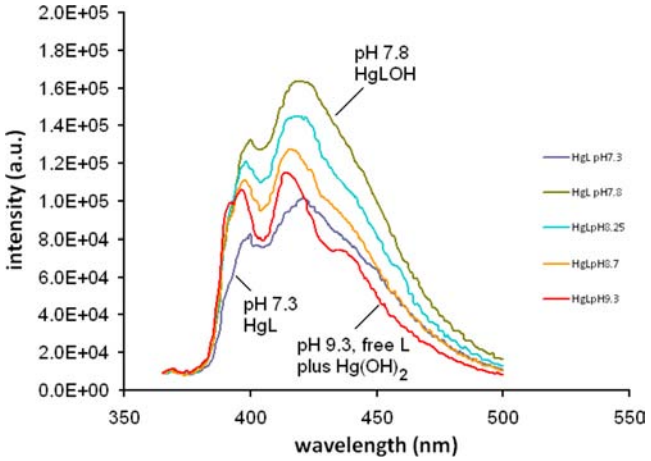

Figure 4. Fluorescence spectra of a 1:1 solution of ADPA and Hg^{II} (5×10^{-6} M) in 50% MeOH at a variety of pH values. From pH 2.91 to 7.25, the spectrum is that of the mercury(II) complex, and above pH 9.0, it is that of the free ADPA ligand. From pH 8 to 9, the more intensely fluorescing species is interpreted as the Hg(ADPA)OH species, whose higher fluorescence intensity is discussed in the text. Wavelength of excitation = 350 nm.

50% MeOH over the pH range 6.4−8.7 are shown in Figure 5. For ADPA in Figure 5, one can calculate the protonation

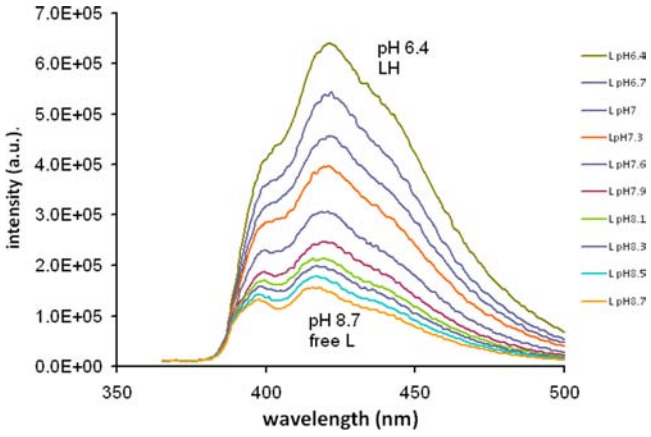

Figure 5. Fluorescence spectra of 5×10^{-6} M ADPA in 50% MeOH over a range of pH values. The fluorescence intensity rises from pH 2.6 to 6.4 (not shown) and then drops from pH 6.4 to 8.7. Variation in the emission intensity as a function of the pH was used to calculate the protonation constants for ADPA in Table 2.

constants $pK_1 = 7.14$ and $pK_2 = 4.70$. The value of $pK_1 = 7.14$ for ADPA is quite close to that of $pK_1 = 7.2$ reported for DPyA in aqueous solution at $\mu = 0.1$,[39] but $pK_2 = 4.7$ for ADPA is considerably higher than $pK_2 = 2.5$ for DPyA in aqueous solution.[39] It is possible that the pK_2 of 4.7 is simply higher than the 2.5 value reported in aqueous solution because of the effect of the 50% MeOH solvent. This seems unlikely because it has been found that several formation constants in water and in 50% MeOH are quite similar.[42] It might be that the pK_2 determined here for ADPA refers to protonation of the excited state of $ADPAH^+$. Protonation constants of excited states of aromatic amines are considerably higher than those for protonation of the ground state.[43] One could not use a pK value that refers to the excited state to calculate a log K_1 value for a metal ion, which refers to the ground state. However, the calculations of log K_1 reported here all refer to equilibria at higher pH values where the pK_2 of ADPA is not involved. It should be borne in mind, however, that the formation constants determined by fluorescence may not be accurate because of interference from excited-state species.

Variation of the emission intensity for the 1:1 Hg^{II}/ADPA solutions in Figure 4 can be analyzed in terms of two equilbria: as the pH is raised, the Hg^{II}/ADPA complex first adds a single OH^- at pH 7.5 to form the $Hg(ADPA)OH^+$ complex, and then at pH 8 and 9, the $Hg(ADPA)OH^+$ complex breaks up into $Hg(OH)_2$ and ADPA. It should be noted that $Hg(OH)_2$ is in solution at the low concentration of 5×10^{-6} M used here and is not a precipitate. The equilibria involved in the Hg^{II}/ADPA system are represented as a species distribution diagram in Figure 6. The constants for the ADPA complexes in Table 2

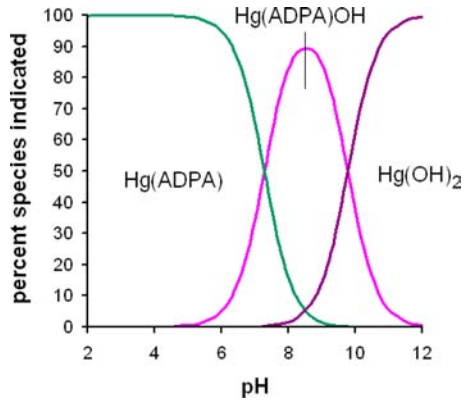

Figure 6. Species distribution diagram for Hg^{II}/ADPA showing the species at greater than 1% of the total Hg as a function of the pH for 5×10^{-6} M ADPA and Hg^{II} in 50% MeOH.

can be seen to be reasonable in comparison with those for the similar DPyA.[39] The log K_1 value for ADPA with Hg^{II} is only approximate because log β_2 for Hg^{II} with OH^- required for calculating log K_1(ADPA) from equilibrium (1) is not known in 50% MeOH, so that the log β_2 (OH^-) value for Hg^{II} in water[39] was used.

The proposed presence of the $Hg(ADPA)OH^+$ species between pH 8 and 9 in the species distribution diagram in Figure 6 correlates with the slightly more intense peak seen in Figure 4 in this pH range. One suggests here that the somewhat more intense peak for the $Hg(ADPA)OH^+$ species is due to dislodging of the π-bonded anthracenyl group from Hg^{II} by the coordinated OH^-, as depicted in Scheme 4.

The response of the fluorescence intensity of the $Hg(ADPA)^{2+}$ complex to coordination of halide ions might be expected to be similar to that of OH^-. A complicating factor is that the collisional quenching ability of anions is largely related to ζ. The collisional quenching due to the heavy I^- anion might be expected to offset the effects of coordination of I^- to Hg^{II} in $Hg(ADPA)^{2+}$, which might, as suggested for OH^- in Scheme 4, be expected to increase the fluorescence intensity. One would expect, on the basis of the magnitude of ζ, that collisional quenching effects would decrease in the order $I^- > Br^- > Cl^- > OH^-$.[43]

In Figure 7 is shown the effect of added Cl^- ion on the fluorescence intensity of the $Hg(ADPA)^{2+}$ complex. Figure 7 suggests that the Cl^- ion also produces an increase in the fluorescence intensity in the $Hg(ADPA)^{2+}$ complex, which, like the increase produced by OH^-, is quite small. The additions of

dx.doi.org/10.1021/ic301380w | Inorg. Chem. 2012, 51, 10904−10915

Scheme 4. Possible Mechanism Whereby Coordination of a Ligand (L) such as Cl^- or OH^- to the $Hg(ADPA)^{2+}$ Complex To Form $Hg(ADPA)Cl^+$ Would Restore the Fluorescence Intensity of the Anthracenyl Group

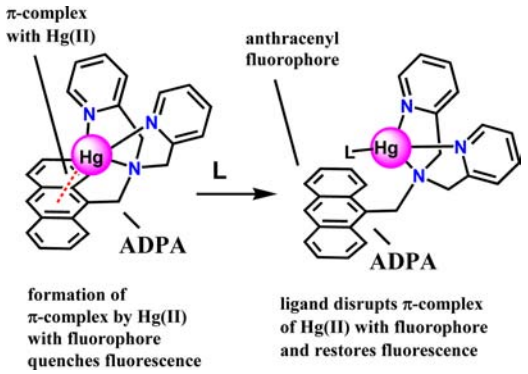

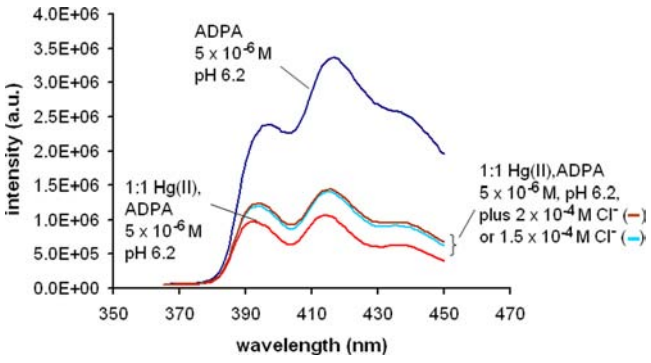

Figure 7. Effect of added Cl^- on the fluorescence of a 5×10^{-6} M Hg^{II}/ADPA complex.

Br^- and I^- to solutions of the $Hg(ADPA)^{2+}$ complex also produce very small increases in the fluorescence intensity.

Structures of ADPA Complexes. *$[Hg(ADPA)Cl_2HgCl_2]$ (1).* The structure of complex **1** is shown in Figure 8. Bond lengths and angles of interest in **1** are given in Table 3. The Hg coordinated to ADPA can be regarded as being approximately octahedrally coordinated, with three N atoms from the ADPA ligand bonded to the Hg atom, plus two Cl^- ions, which are bridging to a second Hg. The sixth coordination site on the Hg atom appears to be occupied by C(16) from the anthracenyl ring, with a Hg–C contact of 3.215 Å. Two types of Hg–C π contacts to the C atoms of the aromatic rings, where the H atom on the C atom is not displaced by the Hg atom, are apparent in the CSD.[28] There are strong π interactions where the Hg–C bonds are fairly short at 2.35 ± 0.07 Å (six structures in the CSD), where the C–C bonds adjacent to the point of attachment to the aromatic ring have been lengthened from values of 1.37 Å typical of phenyl rings to values such as 1.41–1.47 Å and the H atoms attached to the C atom bonded to the Hg atom may be bent away from the Hg atom.[44−47] Most of these short contacts are best described as η^1 bonds, which are somewhat longer than Hg–C bonds to aryl groups, where the Hg atom has displaced a proton (2.07 ± 0.03 Å, 410 structures[28]). Alternatively, more numerous contacts with Hg–C distances averaging 3.37 ± 0.09 Å (74 structures), as typified by the structure of a mercury(II) complex with benzene,[48] are found in the CSD. The controlling factor on whether Hg–C contacts are long or short appears to be the position occupied by the aromatic C atom in the Hg^{II} coordination sphere. It has been pointed out that the coordination geometry of Hg^{II} usually is distorted, so that even where it appears superficially to have a regular coordination geometry with a coordination number higher than 2, two of the more covalently bound donor atoms tend to form two short Hg–L bonds, forming an L–Hg–L bond close to 180°. The remaining, usually more ionically bound donor atoms (L′), form long Hg–L′ bonds and are coordinated at approximately right angles to the L–Hg–L fragment containing the short Hg–L lengths.[49] The short Hg–C contacts to aromatic rings in the vicinity of 2.35 Å all involve contact with an aromatic ring, where any other donor atoms bound to the Hg^{II} atom are few in number, ionically bound, and not occupying the favored linear sites with short Hg–L bonds.[44−47]

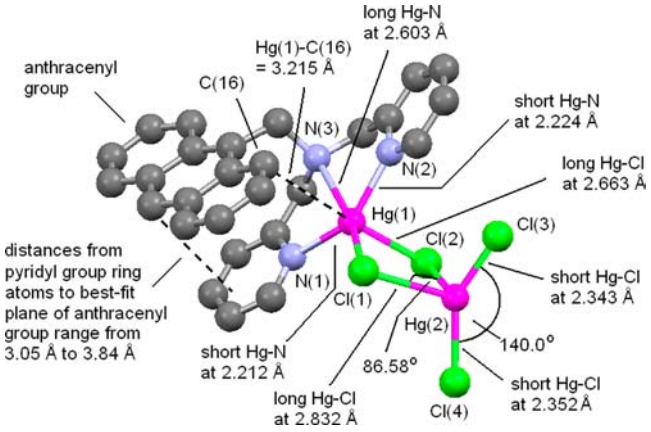

Figure 8. Structure of **1** showing the numbering scheme for atoms coordinated to the two Hg atoms. The drawing shows distortion toward the linear coordination geometry observed for both Hg atoms. Hg(1) shows two short Hg–N bonds, Hg(1)–N(1) = 2.212 Å and Hg(1)–N(2) = 2.224 Å, with an N(1)–Hg(1)–N(2) angle of 143.98°. At roughly right angles to this are a long Hg(1)–N(3) bond of 2.603 Å and two long Hg–Cl bonds: Hg(1)–Cl(1) = 2.502 Å and Hg(1)–Cl(2) = 2.663 Å. Also shown is the Hg(1)–C(16) contact of 3.215 Å, which may be important in quenching the fluorescence of ADPA, as discussed in the text. H atoms are omitted for clarity. The drawing was made with the *Mercury* program available as part of the CSD suite of programs.[28]

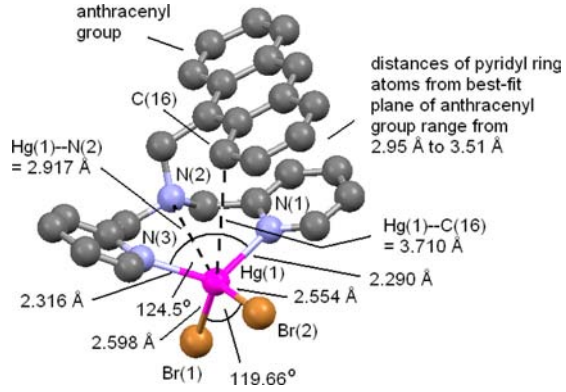

Figure 9. Structure of **2** showing the numbering scheme for atoms coordinated to the Hg atom. The drawing shows the normal Hg–N bond length of 2.310 Å for Hg(1)–N(1) and the long Hg(1)–N(2) contact of 2.917 Å. Also shown is the Hg(1)–C(16) contact of 3.710 Å, which may be too long for quenching of the fluorescence of ADPA, as discussed in the text. H atoms are omitted for clarity. The drawing was made with the *Mercury* program available as part of the CSD suite of programs.[28]

dx.doi.org/10.1021/ic301380w | *Inorg. Chem.* 2012, 51, 10904–10915

Table 3. Bond Lengths and Angles of Interest in 1

Bond Lengths (Å)					
Hg(1)−N(1)	2.212(8)	Hg(1)−N(2)	2.224(8)	Hg(1)−Cl(1)	2.502(3)
Hg(1)−N(3)	2.603(8)	Hg(1)−Cl(2)	2.663(4)	Hg(2)−Cl(3)	2.343(4)
Hg(2)−Cl(4)	2.352(3)	Hg(2)−Cl(2)	2.626(3)	Hg(2)−Cl(1)	2.832(4)
Bond Angles (deg)					
N(1)−Hg(1)−N(2)	144.0(3)		N(1)−Hg(1)−Cl(1)	106.1(2)	
N(2)−Hg(1)−Cl(1)	106.4(2)		N(1)−Hg(1)−N(3)	72.6(3)	
N(2)−Hg(1)−N(3)	71.5(3)		Cl(1)−Hg(1)−N(3)	160.13(18)	
N(1)−Hg(1)−Cl(2)	99.07(19)		N(2)−Hg(1)−Cl(2)	94.2(2)	
Cl(1)−Hg(1)−Cl(2)	92.92(9)		N(3)−Hg(1)−Cl(2)	106.90(18)	
Cl(3)−Hg(2)−Cl(4)	140.52(11)		Cl(3)−Hg(2)−Cl(2)	107.79(10)	
Cl(4)−Hg(2)−Cl(2)	105.66(11)		Cl(3)−Hg(2)−Cl(1)	95.51(11)	
Cl(4)−Hg(2)−Cl(1)	106.88(11)		Cl(2)−Hg(2)−Cl(1)	86.59(8)	
Hg(1)−Cl(1)−Hg(2)	88.01(8)		Hg(2)−Cl(2)−Hg(1)	89.19(8)	

The long Hg−C contacts in the vicinity of 3.37 Å appear to correlate with the aromatic C atoms binding to the Hg atom in the less favored sites away from the two short bonds formed by more strongly and covalently bound donor atoms. This is seen in the structure with long Hg−C π contacts with benzene, where the Hg^{II} ion is otherwise coordinated linearly with two short Hg−C σ bonds. The types of distortions of the geometry around Hg are well illustrated by the structure of **1**.

Figure 10 shows the relationship between the Hg−Cl bond lengths and Cl−Hg−Cl bond angles for four-coordinate

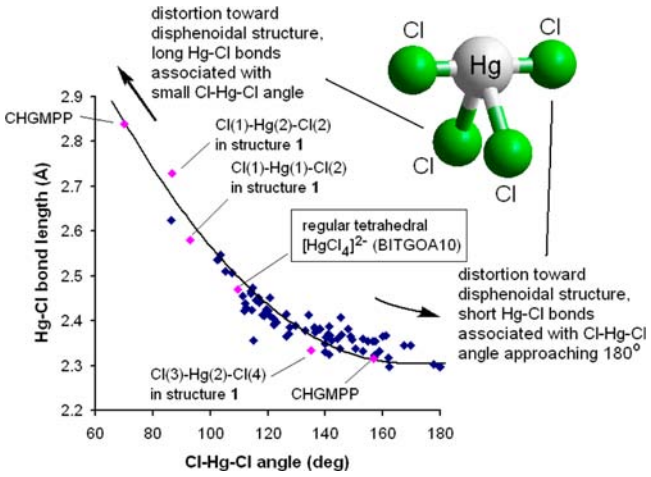

Figure 10. Relationship between average Hg−Cl bond lengths and Cl−Hg−Cl angles in mercury(II) complexes with HgN_2Cl_2 donor sets (dark-blue points) from 74 structures in the CSD ($R < 0.10$).[28] Also included in the diagram (pink points) are Hg−Cl bond lengths and angles from structure **1**, as well as examples of the Hg−Cl bond lengths and Cl−Hg−Cl bond angles from a regular $[HgCl_4]^{2-}$ complex anion (CSD refcode BITGOA10) and a highly distorted $[HgCl_4]^{2-}$ complex anion (CSD refcode CHGMPP). For CHGMPP, there are two long Hg−Cl bonds and two short Hg−Cl bonds, and the Cl−Hg−Cl angles for CHGMPP in the diagram refer to the angles subtended by the two long bonds and two short bonds.

mercury(II) complexes with N_2Cl_2 donor sets. At one extreme of the relationship, with Cl−Hg−Cl angles approaching 180°, the Hg^{II} atom adopts a saw-horse, or disphenoidal, type of structure, with the two Cl atoms occupying the favored short Hg−Cl bonds of about 2.3 Å. In these structures, the N-donor atoms bind at right angles to the ClHgCl substructure and form long Hg−N bonds with small N−Hg−N angles. At the other extreme, the N-donor atoms occupy the favored linear coordination sites, the Hg−Cl bonds are long, approaching 2.8 Å, and the Cl−Hg−Cl angle is small, approaching 70°. In the center of the relationship, we have placed the Hg−Cl lengths (2.47 Å) and Cl−Hg−Cl bond angles (~109°) for a structure containing a close to regular tetrahedral $[HgCl_4]^{2-}$ anion (CSD code BITGOA10).[50] Also included in Figure 10 are the Hg−Cl lengths and Cl−Hg−Cl angles for a highly distorted $[HgCl_4]^{2-}$ anion (CSD code CHGMPP).[51]

The Hg(2) atom in structure **1** has four Cl atoms coordinated to it, and the tendency toward a saw-horse type of geometry around Hg(2) seen in Figure 8 has Hg−Cl lengths and angles much as expected from the relationship in Figure 10. Also included in Figure 10 are the long Hg(1)−Cl bonds, with the accompanying small Cl−Hg−Cl angle, which is much as would be expected from the relationship for the $HgCl_2N_2$ complexes. The long Hg(1)−N(3) bond to the saturated N-donor atom of the ADPA ligand in **1** can thus be understood as originating from the fact that it occupies a less favored coordination position at right angles to the short Hg(1)−N(1) and Hg(1)−N(2) bonds. The long Hg(1)−C(16) contact to the anthracenyl group thus also falls into this category of Hg−L interactions. In the structure where Hg^{II} forms long contacts with benzene, it is suggested that these long Hg−C contacts of 3.41−3.46 Å are indeed bonds,[49] and it seems likely here that the Hg(1)−C(16) contact of 3.215 Å might be evidence for the type of Hg−C π contact suggested by Czarnik et al. as being responsible for the quenching of tethered fluorophores by Hg^{II}.[21]

*[Hg(ADPA)Br$_2$] (**2**).* The structure of **2** is shown in Figure 9, and bond lengths and angles of interest are given in Table 4. The Hg atom in **2** is essentially four-coordinate, with a flattened tetrahedral geometry. As might be expected, the more covalently bound Br^- ions cause the coordination geometry of the Hg ion to be more nearly tetrahedral than is the case for

Table 4. Bond Lengths and Angles of Interest in 2

Bond Lengths (Å)			
Hg(1)−N(1)	2.289(3)	Hg(1)−N(3)	2.317(3)
Hg(1)−Br(2)	2.5538(4)	Hg(1)−Br(1)	2.5985(4)
Bond Angles (deg)			
N(1)−Hg(1)−N(3)	124.50(12)	N(1)−Hg(1)−Br(2)	105.85(8)
N(3)−Hg(1)−Br(2)	101.92(8)	N(1)−Hg(1)−Br(1)	101.46(8)
N(3)−Hg(1)−Br(1)	104.92(8)	Br(2)−Hg(1)−Br(1)	119.662(16)

dx.doi.org/10.1021/ic301380w | *Inorg. Chem.* 2012, 51, 10904−10915

the Cl^- ions in **1**. The amount of distortion away from the tetrahedral geometry found in mercury(II) complexes in the CSD with an N_2Br_2 donor set for Br−Hg−Br angles ranges from of 114° to 160°, compared to a range of 70−180° for Cl−Hg−Cl angles in mercury(II) complexes with an N_2Cl_2 donor set shown in Figure 9. With the coordinated Br^- ligands in **2**, one finds that, in contrast to $[Hg(ADPA)Cl_2]$, the anthracenyl group has moved away from the Hg to the point where the Hg−C(16) contact is now 3.710 Å, probably too long to be a contact that might interfere with the fluorescence of ADPA. At the same time, the Hg(1)−N(2) contact to the central saturated N-donor atom of ADPA has been lengthened to 2.917 Å. The lone pair on N(2) may therefore still be of high enough energy to cause a PET effect, as outlined in Scheme 1, and so quench the fluorescence that might be expected from the long Hg−C(16) contact in **2**.

*[Cu(ADPA)(NO$_3$)$_2$] (**3**).* The structure of **3** is shown in Figure 11, and bond lengths and angles of interest are given in Table 5.

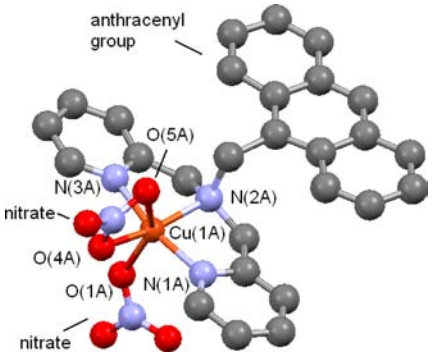

Figure 11. Structure of complex **3**, showing the numbering scheme for atoms coordinated to the Cu atom. H atoms are omitted for clarity. The drawing was made with the *Mercury* program available as part of the CSD suite of programs.[28]

Table 5. Bond Lengths and Angles of Interest in 3

Bond Lengths (Å)			
Cu(1A)−N(1A)	1.9733(17)	Cu(1A)−N(3A)	1.9809(17)
Cu(1A)−O(4A)	2.0183(13)	Cu(1A)−N(2A)	2.0482(16)
Cu(1A)−O(1A)	2.2618(14)		
Bond Angles (deg)			
N(1A)−Cu(1A)−N(3A)	166.64(7)	N(1A)−Cu(1A)−O(4A)	96.49(6)
N(3A)−Cu(1A)−O(4A)	96.44(6)	N(1A)−Cu(1A)−N(2A)	83.61(6)
N(3A)−Cu(1A)−N(2A)	83.03(6)	O(4A)−Cu(1A)−N(2A)	163.90(6)
N(1A)−Cu(1A)−O(1A)	100.16(6)	N(3A)−Cu(1A)−O(1A)	81.69(6)

The Cu^{II} atom in **3** has the usual tetragonally distorted structure for apparent six-coordination, with the three N-donor atoms of the ADPA ligand coordinated in the plane of the Cu^{II} atom, with the fourth position in the plane occupied by O(4) from a chelating nitrate. The in-plane bonds to Cu^{II} are as usual quite short: Cu(1A)−N(1A) = 1.9733(17) Å; Cu(1A)−N(3A) = 1.9809(17) Å; Cu(1A)−O(4A) = 2.0183(13) Å; Cu(1A)−N(2A) = 2.0482(16) Å. The chelating nitrate has its second O-donor atom coordinated to the Cu^{II} atom in an axial position with the long Cu(1A)−O(5A) contact of 2.518(2) Å. The second nitrate is coordinated in an axial position to the Cu^{II} atom in a unidentate fashion, with the fairly long Cu(1A)−O(1A) bond of 2.2618(14) Å. The structure of **3** shows how, with the Cu^{II}/ADPA complex, which is also illustrated by a similar structure with a ClO_4^- counterion,[52] the Cu^{II} atom does not interact with the anthracenyl aromatic ring. A similar structure of the Ni^{II}/ADPA complex also does not show any interaction of the Ni^{II} atom with the aromatic ring.[53] The structure of complex **3** does suggest that the effects of the paramagnetic Cu^{II} ion in causing quenching of the fluorescence of the anthracenyl group in ligands such as ADPA may not require a close approach of the Cu^{II} atom to the fluorophore. Other structures in which Cu^{II} and an anthracenyl group are present have the anthracenyl group quite close to the Cu^{II} atom, with the closest C atom from the anthracenyl group giving a Cu−C contact of 2.95 Å,[54] so that it is not quite clear that the effect always does not involve fairly close contact of the Cu^{II} atom with a C atom of the fluorophore when in solution.

Examining some turn-on sensors for Hg^{II} reported in the literature, one notes that these involve structures where it seems probable that the Hg^{II} atom should be held well clear of the fluorophore, and covalently binding donor atoms are present that should limit the strength of interaction of the Hg^{II} atom with the fluorophore. Thus, in the fluorescein-based sensor (**L2**) reported by Nolan and Lippard,[55] the ligating group intended to bind the Hg^{II} atom has an NS_2 donor set (Scheme 5). In a rather similar ligand (**L3**), the Hg^{II} atom is

Scheme 5. Some Turn-on Fluorescent Sensors for Hg^{II} in Aqueous Solution Reported in the Literature[a]

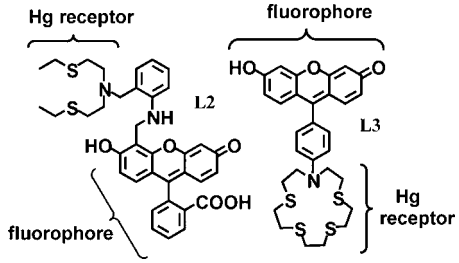

[a] **L2** and **L3** are from refs 55 and 58, respectively.

bound by a macrocycle with an NS_5 donor set.[56] The principle that leads to a turn-on sensor that can be deduced from these ligands is that the presence of highly covalent S-donor atoms in the Hg^{II} receptor ligand will greatly reduce the tendency of the Hg^{II} atom to interact with the fluorophore, as seen for the Br-donor atoms in structure **2**. The role of secondary ligands such as Br^- in weakening the interaction of Hg^{II} with the fluorophore indicated by structure **2** suggests that great care should be exercised in evaluating sensors for Hg^{II} in acetonitrile[57] as a solvent. This point is particularly made by a structure of Hg^{II} coordinated with an N_4S_2 donor set,[58] where a coordinated acetonitrile occupies one of the two favored linear N−Hg−N binding sites with short Hg−N bonds, even in competition with the covalently binding S-donor atoms. This suggests that coordinated acetonitrile might affect the fluorescence properties of the mercury(II) complex and limit interaction with the fluorophore in the same way as that seen for the Br^- ligand in structure **2**. Fluorescence results for Hg^{II} sensors obtained in acetonitrile might therefore not apply to their potential use in aqueous solution.

DFT Calculations. The structure of $[Hg(ADPA)(H_2O)_2]^{2+}$ in aqueous solution (Figure 12) was optimized with a PCM, and the bond lengths and angles of interest are given in Table

dx.doi.org/10.1021/ic301380w | *Inorg. Chem.* 2012, 51, 10904−10915

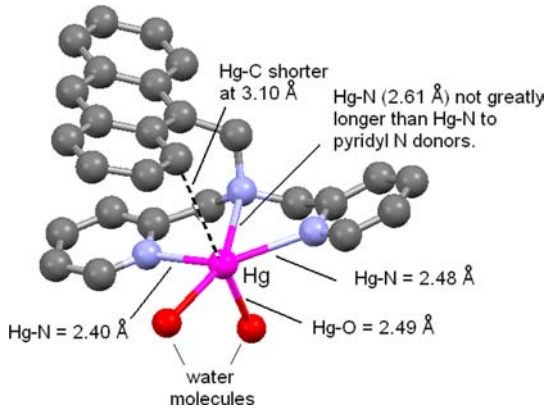

Figure 12. DFT-generated structure of $[Hg(ADPA)(H_2O)_2]^{2+}$, showing the shorter Hg−C contact to the anthracenyl fluorophore and to the saturated N-donor atom of the dipicolylamine portion of the ligand. H atoms are omitted for clarity. The drawing was made with the *Mercury* program available as part of the CSD suite of programs.[28].

6. The optimized structure includes two explicit water molecules coordinated to Hg^{II}, one on the same plane as the N atoms (equatorial position) and another positioned at the opposite side of the anthracenyl group (axial position). The structural parameters of $[Hg(ADPA)(H_2O)_2]$ are overall in agreement with those of the ADPA complex part of **1** obtained from X-ray crystallography. The Hg−O bond lengths are slightly shorter than the Hg−Cl distances in $Hg(ADPA)Cl_2HgCl_2]$, which is to be expected from the shorter covalent radius of O compared to Cl.

Table 6. Bond Lengths and Angles of Interest in $[Hg(ADPA)(H_2O)_2]$ Obtained from the DFT/B3LYP/SV(P)/Lanl2DZ Basis-Set Calculation with PCM[a]

Bond Lengths (Å)					
Hg(1)−N(1)	2.466	Hg(1)−N(2)	2.476	Hg(1)−O(1)	2.400
Hg(1)−N(3)	2.610	Hg(1)−O(2)	2.485		
Bond Angles (deg)					
N(1)−Hg(1)−N(2)	140.4	N(1)−Hg(1)−O(1)	83.7		
N(2)−Hg(1)−O(1)	135.9	N(1)−Hg(1)−N(3)	70.1		
N(2)−Hg(1)−N(3)	70.5	O(1)−Hg(1)−N(3)	153.2		
N(1)−Hg(1)−O(2)	82.8	N(2)−Hg(1)−O(2)	91.3		
Cl(1)−Hg(1)−O(2)	95.9	N(3)−Hg(1)−O(2)	86.6		

[a]The numbering scheme is the same as that in Figure 8, except that O(1) refers to the O atom of the water on the same plane as the N atoms (equatorial), whereas O(2) refers to the O atom in the axial position.

As expected from the X-ray structure of **1**, a significant interaction between anthracenyl C(16) and Hg is observed in $[Hg(ADPA)(H_2O)_2]$, which is reflected in the shorter Hg−C(16) distance (3.11 Å) than that of crystal **1**. The Hg−C(16) bond length in $[Hg(ADPA)(H_2O)_2]$ is close to that of long Hg−C contacts (3.37 Å), typically seen in the structures of mercury(II) complexes with benzene.[48] Bond-order analysis shows that Hg−C(16) has a bond order of 0.085, which is not negligible. This is within the same range as the bond orders of C−C and C−N π interactions within the aromatic picolyl group of ADPA. However, the C−C and C−N distances across the picolyl group are much shorter, on the order of 2.76−2.80 Å, than that of Hg−C(16) in $[Hg(ADPA)(H_2O)_2]$, which shows the effectiveness of the Hg−C(16) interaction. The interactions between Hg and nearby N and O atoms have bond orders in the range of 0.29−0.36, but the bond lengths are much shorter, at 2.40−2.61 Å.

Upon the introduction of halogen anions into the $[Hg(ADPA)(H_2O)_2]$ system and replacement of the water molecules, in the DFT-generated structures, the Hg−C(16) distance increases drastically. As shown in Table 7, the Hg−C(16) distance in $[Hg(ADPA)Cl_2]$ increases to 4.086 Å and the distance continues to increase as larger halogen atoms replace the water molecules. The same trend was observed in the X-ray structures of **1** and **2**, although the X-ray crystal structures have shorter Hg−C(16) bond lengths than the corresponding structures in aqueous solution (Table 7). There is also noticeable structural change in the Hg^{II}/ADPA systems. In particular, as the halogen atoms pull the Hg atom away from the fluorophore, two picolyl arms of ADPA are lifted up toward the anthracenyl group. The introduction of hydroxide ions has a similar impact on the structure of Hg(ADPA) systems as well. When the water molecule at the equatorial position is replaced by a hydroxide ion, the Hg−C(16) distance increases to 3.27 Å. The $[Hg(ADPA)OH(H_2O)]$ structure with OH^- at the axial position has an almost identical energy value (only 0.36 kcal·mol^{-1} higher), but the Hg−C(16) distance is much longer, at 4.20 Å. Therefore, the hydroxide ion can pull the Hg atom away from the anthracenyl group more effectively when it coordinates to Hg at the axial position. Because of such a small energy difference, both structures are expected to be present at room temperature. When both water molecules are replaced by hydroxide ions, the Hg−C(16) distance becomes 4.09 Å, which is the same as that in $[Hg(ADPA)Cl_2]$. Therefore, it is expected that the ability of OH^- and Cl^- to disengage Hg from the antracenyl group is comparable.

The importance of the Hg−fluorophore interaction is also manifested in the electronic structures of $[Hg(ADPA)(H_2O)_2]^{2+}$. The excitation energies, oscillator strengths, and compositions of the singlet excited states obtained from TDDFT calculations with the optimized ground-state geometry are reported in Table 8. The frontier orbitals (HOMO, LUMO, and LUMO+1) of $[Hg(ADPA)(H_2O)_2]$ are also shown in Figure 13. The $S_0 \rightarrow S_1$ transition is allowed with a rather small oscillator strength. The nature of this excitation is mostly a HOMO → LUMO transition, but the HOMO → LUMO+1 transition is not negligible (11% contribution). Interestingly, LUMO and LUMO+1 look quite similar, and none of them is

Table 7. Minimum Distance (Å) between Hg and the Fluorophore for the Optimized Geometries of $[Hg(ADPA)X_2]$ (X = H_2O, Cl, Br, and I) Compounds[a]

$Hg(ADPA)(H_2O)_2^{2+}$	$Hg(ADPA)Cl_2$	$Hg(ADPA)Br_2$	$Hg(ADPA)I_2$	$Hg(ADPA)OH(H_2O)^+$	$Hg(ADPA)(OH)_2$
3.109	4.086	4.186	4.341	3.267 (4.196)	4.085

[a]Geometry optimizations were performed using a DFT/B3LYP/SV(P)/Lanl2DZ basis set with the PCM solvation model. For $[Hg(ADPA)OH(H_2O)]$, the number in parentheses is the Hg−C(16) distance for the structure with the OH located at the axial position.

dx.doi.org/10.1021/ic301380w | *Inorg. Chem.* 2012, 51, 10904−10915

Table 8. Electronic Excitation Energies (eV), Oscillator Strengths (f), and Configurations of Selected Low-Lying Excited State of [Hg(ADPA)X_2] (X = H_2O, Cl, Br, and I) Compounds Obtained from the TDDFT/B3LYP/SVP(P)/Lanl2DZ Basis Set with a PCM Solvation Model[a]

compound	transition	excitation energy (eV)	f	composition[b]	% contribution
$Hg(ADPA)(H_2O)_2^{2+}$	$S_0 \rightarrow S_1$	2.815	0.07273	H → L	87.8
				H → L+1	11.6
	$S_0 \rightarrow S_2$	3.068	0.05680	H → L+1	86.5
				H → L	11.2
$Hg(ADPA)OH(H_2O)^+$	$S_0 \rightarrow S_1$	3.035	0.11301	H → L	98.4
$Hg(ADPA)(OH)_2$	$S_0 \rightarrow S_1$	3.065	0.10498	H → L	98.2
$Hg(ADPA)Cl_2$	$S_0 \rightarrow S_1$	3.054	0.11085	H → L	98.1
$Hg(ADPA)Br_2$	$S_0 \rightarrow S_1$	3.055	0.11664	H → L	98.0
$Hg(ADPA)I_2$	$S_0 \rightarrow S_1$	3.047	0.11004	H → L	94.6
				H → L+1	3.7

[a]TDDFT calculations were performed with the optimized ground-state geometries. [b]H is HOMO, and L is LUMO.

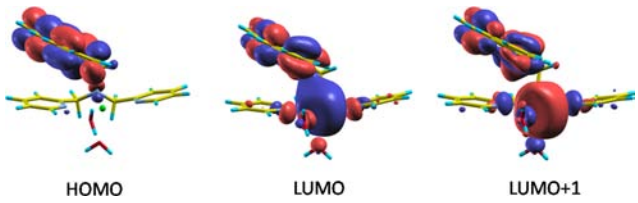

Figure 13. Frontier orbitals of the ground state [Hg(ADPA)$(H_2O)_2$] obtained from the DFT/B3LYP/SVP(P)/Lanl2DZ basis set with a PCM solvation model.

exclusively localized in the fluorophore (Figure 13). Instead, they have a substantial contribution from Hg, which suggests that the $S_0 \rightarrow S_1$ transition should be regarded as a charge transfer to Hg. The next-allowed singlet excitation ($S_0 \rightarrow S_2$) has similar characteristics, mostly a HOMO → LUMO+1 transition with a nonnegligible contribution from the HOMO → LUMO excitation. As depicted in Scheme 1, a PET process followed by fluorescence quenching occurs when the receptor HOMO is located above the fluorophore HOMO. The receptor electrons then drop down to the fluorophore HOMO, blocking the excited-state electrons from falling back to the ground state. Metal coordination prevents electron transfer from the receptor to the fluorophore and restores the fluorescence (CHEF). Metal-induced fluorescence quenching may occur in opposite ways. Metal chelation can lower the receptor LUMO below the fluorophore LUMO, which allows electron relaxation from the fluorophore LUMO to the receptor LUMO after the initial HOMO → LUMO excitation of the fluorophore. Examples of this are the BODIPY (Figure 1) sensors.[59] However, Hg-induced fluorescence quenching seen in [Hg(ADPA)$(H_2O)_2$] does not fit into a simple picture described above. In fact, a significant Hg–anthracenyl group interaction does not allow clear identification of whether some molecular orbitals belong to the receptor or to the fluorophore. In the case of [Hg(ADPA)$(H_2O)_2$], it is possible that the electrons excited to LUMO+1 relax to LUMO during the reorganization of the system to the vibrational ground state of the S_1 surface. If the subsequent $S_1 \rightarrow S_0$ transition has a more substantial charge-transfer character (from Hg to the anthracenyl group) than that of absorption, fluorescence may be effectively quenched. More detailed calculations, including excited-state geometry optimization, are currently underway to verify such a possibility.

When halogen anions are introduced, the absorption/emission mechanisms seem to be simplified due to the lack of a Hg–anthracenyl group interaction. As shown in Table 8 and Figure 14, the absorptions occur exclusively between the

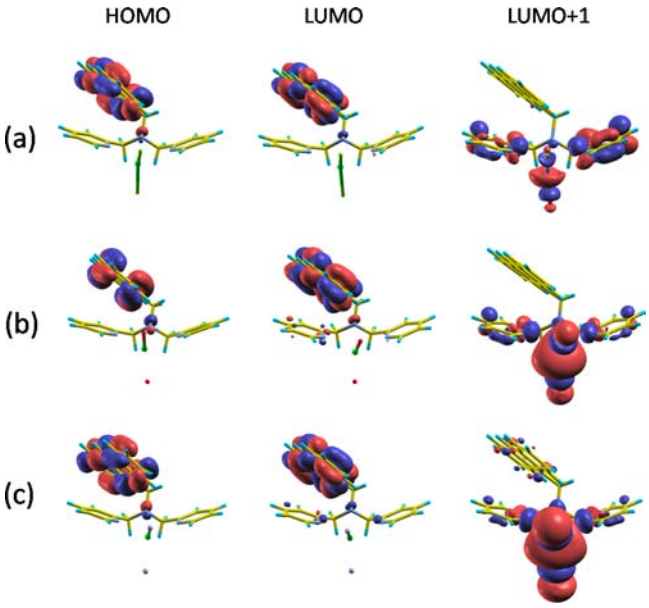

Figure 14. Frontier orbitals of the ground state [Hg(ADPA)$(Cl)_2$] (a), [Hg(ADPA)$(Br)_2$] (b), and [Hg(ADPA)$(I)_2$] (c) obtained from the DFT/B3LYP/SVP(P)/Lanl2DZ basis set with a PCM solvation model.

HOMO and LUMO of the fluorophore. In the case of [Hg(ADPA)X_2] (X = Cl, Br, and I), the HOMO of the receptor is located far below the HOMO of the fluorophore, and electron transfer from the receptor to the fluorophore (Scheme 1) is not possible. Relaxation of the excited-state electrons to the LUMO of the receptor is not allowed either because the receptor LUMO (LUMO+1 in Figure 14) is located above the LUMO of the fluorophore. Therefore, fluorescence is expected to be restored (at least partially) with halogen atoms coordinated to Hg, which is consistent with the experimental observation (Figure 7). A similar behavior is also observed for the complexes with OH^-. Even with only one hydroxide ion coordinated to Hg, the HOMO → LUMO transition is contained within the fluorophore (molecular orbitals are not shown). There is no receptor state around the fluorophore LUMO with a lower energy value, which indicates that excited-state electrons can drop back to the ground state

dx.doi.org/10.1021/ic301380w | Inorg. Chem. 2012, 51, 10904–10915

and the fluorescence will be restored. This supports our experimental observation that the fluorescence intensity of [Hg(ADPA)] increases with pH (Figure 4).

CONCLUSIONS

(1) The proposal[22] that Hg^{II} quenches the fluorescence of sensors that possess a formally noncoordinating, "tethered", fluorophore, such as an anthracenyl group, by forming π bonds to C atoms of the fluorophore is supported by the structure of **1** reported here and by DFT calculations. (2) An additional factor is that coordination of more covalently binding ligands to Hg^{II}, such as Cl^-, Br^-, and I^-, as supported by crystallography and DFT calculations, tends to lengthen the Hg−N bond to the saturated N-donor atom of the dipicolylamine part of the ADPA ligand. This is strongly evident in the structure of **2**. A CHEF effect depends on the metal-ion binding to the N-donor atoms of the ligand sufficiently strongly to lower the energy of the lone pair of the N-donor atom, which otherwise quenches fluorescence by a PET effect. Greatly weakening the Hg−N bond to the saturated N-donor atom of the ADPA ligand thus leaves the lone pair on this N-donor atom at a high enough energy to quench the expected CHEF effect. This tendency of Hg^{II} to form short bonds to only a few of the donor atoms provided by a potential sensor may be a largely unconsidered factor that contributes in many cases to the inability of Hg^{II} to produce a CHEF effect. It leaves the lone pairs on the donor atoms that form long weak bonds at sufficiently high energy to produce a PET effect and so quench fluorescence. (3) It had been expected that binding ligands such as Cl^- or Br^- to Hg^{II} in its ADPA complex would weaken its π interaction with the anthracenyl fluorophore and thus produce enhanced fluorescence. It turns out that such covalently bound ligands as Cl^- and Br^- also weaken the interaction of Hg^{II} with the saturated N atom of ADPA, thus allowing quenching by a PET effect. It does appear, however, that bound Cl^- and OH^- do produce a weak increase in fluorescence, where weakening of the Hg−N bond, which produces a quenching CHEF effect, is somewhat offset by weakening of the π interaction of Hg^{II} with the fluorophore. (4) Mercury(II) complexes tend to be distorted by the formation of short bonds to more covalently bound donor atoms and long bonds to more ionically bound donor atoms. In the case of the Hg^{II}/ADPA complexes, as supported by both crystallography and DFT calculations, this distortion becomes more extreme as more covalently bound ligands bind to the Hg^{II}/ADPA complex along the series $H_2O < Cl^- < Br^- < I^-$. (5) In the design of turn-on sensors for Hg^{II}, a good strategy appears to be to have covalently binding donor atoms, particularly S-donor atoms, on the chelating part of the sensor. These covalently bound donor atoms weaken the interaction of Hg^{II} with the fluorophore, which otherwise quenches the fluorescence. (6) DFT calculations suggest that the quenching effect of Hg^{II} in its ADPA complexes is due to covalent π interaction of Hg^{II} with the fluorophore, which greatly decreases the electronic transition probability from the excited state to the ground state.

AUTHOR INFORMATION

Corresponding Author

*E-mail: hancockr@uncw.edu.

Notes

The authors declare no competing financial interest.

ACKNOWLEDGMENTS

The authors thank the University of North Carolina, Wilmington and the Department of Energy (Grant DE-FG07-07ID14896) for generous support of this work.

REFERENCES

(1) Sigel, A.; Sigel, H.; Sigel, R. K. O. *Metal Ions in Life Sciences. Neurodegenerative Diseases and Metal Ions*; John Wiley & Sons: Chichester, U.K., 2006; Vol. *1*.
(2) Nordberg, G. F.; Fowler, B. A.; Nordberg, M.; Friberg, L. *Handbook on the Toxicology of Metals*, 3rd ed.; Elsevier Inc.: New York, 2007.
(3) Vernet, P. *Heavy Metals in the Environment*; Elsevier: New York, 1991.
(4) Bencini, A.; Bernardo, M. A.; Bianchi, A.; Garcia-Espana, E.; Giorgi, C.; Luis, S.; Pina, F.; Valtancoli, B. *Adv. Supramol. Chem.* **2002**, *8*, 79.
(5) Hilderbrand, S. A.; Lim, M. H.; Lippard, S. J. *Top. Fluoresc. Spectrosc.* **2005**, *9*, 163.
(6) Thompson, R. B.; Bozym, R. A.; Cramer, M. L.; Stoddard, A. K.; Westerberg, N. M.; Fierke, C. A. *Fluoresc. Sens. Biosens.* **2006**, 107.
(7) Parker, D.; Williams, J. A. G. *Metal Ions Biol. Syst.* **2003**, *40*, 233.
(8) Burdette, S. C.; Lippard, S. J. *Coord. Chem. Rev.* **2001**, *216−217*, 333.
(9) Valeur, B.; Leray, I. *Coord. Chem. Rev.* **2000**, *205*, 3.
(10) Czarnik, A. W. *Trends Org. Chem.* **1993**, *4*, 123.
(11) Mason, W. T. Fluorescent and luminescent probes for biological activity. In *Biological Techniques*; Sattelle, D. B., Ed.; Academic Press: San Diego, CA, 1999.
(12) Xu, Z.; Yoon, J.; Spring, D. R. *Chem. Soc. Rev.* **2010**, *39*, 1996.
(13) Zhang, J. F.; Kim, J. S. *Anal. Sci.* **2009**, *25*, 1271.
(14) de Silva, A. P.; Gunaratne, H. Q. N.; Gunnlaugsson, T.; Huxley, A. J. M.; McCoy, C. P.; Rademacher, J. T.; Rice, T. E. *Chem. Rev.* **1997**, *97*, 1515.
(15) McClure, D. S. *J. Chem. Phys.* **1949**, *17*, 905.
(16) Solovyov, K. N.; Borisevich, E. A. *Phys. Uspekii* **2005**, *48*, 231.
(17) (a) Bazzicalupi, C.; Bencini, A.; Bianchi, A.; Giorgi, C.; Fusi, V.; Valtancoli, B.; Bernado, M. A.; Pina, F. *Inorg. Chem.* **1999**, *38*, 3806. (b) Bazzicalupi, C.; Bencini, A.; Berni, E.; Bianchi, A.; Fornasari, P.; Giorgi, C.; Valtancoli, B. *Eur. J. Inorg. Chem.* **2003**, 1974.
(18) (a) Mikata, Y.; Wakamatsu, W.; Kawamura, A.; Yamanaka, N.; Yano, S.; Odani, A.; Morihiro, K.; Tamotsu, S. *Inorg. Chem.* **2006**, *45*, 9262. (b) Mikata, Y.; Wakamatsu, M.; Yano, S. *Dalton Trans.* **2005**, 545. (c) Mikata, Y.; Yamanaka, N.; Yamashita, A.; Shigenobu, Y. *Inorg. Chem.* **2008**, *47*, 2008.
(19) Gan, W.; Jones, S. B.; Reibenspies, J. H.; Hancock, R. D. *Inorg. Chim. Acta* **2005**, *358*, 3958.
(20) Williams, N. J.; Gan, W.; Reibenspies, J. H.; Hancock, R. D. *Inorg. Chem.* **2009**, *48*, 1407.
(21) Cockrell, G. M.; Zhang, G.; VanDerveer, D. G.; Thummel, R. P.; Hancock, R. D. *J. Am. Chem. Soc.* **2008**, *130*, 1420.
(22) Yoon, J.; Ohler, N. E.; Vance, D. H.; Aumiller, W. D.; Czarnik, A. W. *Tetrahedron Lett.* **1997**, *38*, 3845.
(23) Williams, N. J.; Dean, N. E.; VanDerveer, D. G.; Luckay, R. C.; Hancock, R. D. *Inorg. Chem.* **2009**, *48*, 7853.
(24) De Silva, S. A.; Zavaleta, A.; Baron, D. E.; Allam, O.; Isidor, E. V.; Kashimura, N.; Percarpio, J. M. *Tetrahedron Lett.* **1997**, *38*, 2237.
(25) *HyperChem*, version 8.0; Hypercube, Inc.: Waterloo, Ontario, Canada; 2007.
(26) Ojida, A.; Mito-oKa, Y.; Inoue, M.; Hamachi, I. *J. Am. Chem. Soc.* **2002**, *124*, 6256.
(27) Hedges, J. I.; Stern, J. H. *Limnol. Oceanogr.* **1984**, *29*, 663.
(28) *Cambridge Structural Database*; Cambridge Crystallographic Data Centre: Cambridge, U.K.; 2012.
(29) Gabe, E. J.; Le Page, Y.; Charland, J.-P.; Lee, F. L.; White, P. S. *J. Appl. Crystallogr.* **1989**, *22*, 384.
(30) *FluorEssence*, version 2.1; Horiba Jobin Yvon, Inc.: Edison, NJ, 2006.

(31) Schmidt, M. W.; Baldridge, K. K.; Boatz, J. A.; Elbert, S. T.; Gordon, M. S.; Jensen, J. H.; Koseki, S.; Matsunaga, N.; Nguyen, K. A.; Su, S.; Windus, T. L.; Dupuis, M.; Montgomery, J. A. *J. Comput. Chem.* **1993**, *14*, 1347.
(32) Lee, C.; Yang, W.; Parr, R. G. *Phys. Rev. B* **1988**, *37*, 785.
(33) Becke, A. D. *J. Chem. Phys.* **1993**, *98*, 5648.
(34) Weigend, F.; Ahlrichs, R. *Phys. Chem. Chem. Phys.* **2005**, *7*, 3297.
(35) Hay, P. J.; Wadt, W. R. *J. Chem. Phys.* **1985**, *82*, 270.
(36) Hay, P. J.; Wadt, W. R. *J. Chem. Phys.* **1985**, *82*, 284.
(37) Hay, P. J.; Wadt, W. R. *J. Chem. Phys.* **1985**, *82*, 299.
(38) Billo, E. J. *EXCEL for Chemists*; Wiley-VCH: New York, 2001.
(39) Martell, A. E.; Smith, R. M. *Critical Stability Constant Database*; National Institute of Science and Technology (NIST): Gaithersburg, MD, 2003; Vol. *46*.
(40) Hamilton, J. M.; Whitehead, J. R.; Williams, N. J.; Thummel, R. P.; Hancock., R. D. *Inorg. Chem.* **2011**, *50*, 3785−3790.
(41) Hamilton, J. M.; Anhorn, M. J.; Oscarson, K. A.; Reibenspies, J. H.; Hancock, R. D. *Inorg. Chem.* **2011**, *50*, 2764−2770.
(42) Miguirditchian, M.; Guillaneux, D.; Guillaumont, D.; Moisy, P.; Madic, C.; Jensen, M. P.; Nash, K. L. *Inorg. Chem.* **2005**, *44*, 1404.
(43) Lakowicz, J. R. *Principles of Fluorescence Spectroscopy*, 2nd ed.; Plenum: New York, 1999; pp 211 and 516.
(44) Borovik, A. S.; Bott, S. G.; Barron, A. R. *Angew. Chem., Int. Ed.* **2000**, *39*, 4117.
(45) Borovik, A. S.; Bott, S. G.; Barron, A. R. *J. Am. Chem. Soc.* **2001**, *123*, 11219.
(46) Marsh, R. E.; Clemente, D. A. *Inorg. Chim. Acta* **2007**, *360*, 4017.
(47) Lau, W.; Huffman, J. C.; Kochi, J. K. *J. Am. Chem. Soc.* **1982**, *104*, 5515.
(48) Tsunoda, M.; Gabbaï, F. P. *J. Am. Chem. Soc.* **2000**, *122*, 8335 (trimer plus benzene).
(49) Hancock, R. D.; Reibenspies, J. H.; Maumela, H. *Inorg. Chem.* **2004**, *43*, 2981.
(50) Salah, A. B.; Bats, J. W.; Kalus, R.; Fuess, H.; Daoud, A. Z. *Anorg. Allg. Chem.* **1982**, *493*, 178.
(51) Baker, R. W.; Braithwaite, M. J.; Nyholm, R. S. *J. Chem. Soc., Dalton Trans.* **1972**, 1924.
(52) Antonioli, B.; Buchner, B.; Clegg, J. K.; Gloe, K.; Gloe, K.; Gotzke, L.; Heine, A.; Jager, A.; Jolliffe, K. A.; Kataeva, O.; Kataev, V.; Klingeler, R.; Krause, T.; Lindoy, L. F.; Popa, A.; Seichter, W.; Wenzel, M. *Dalton Trans.* **2009**, 4795.
(53) Gotzke, L.; Gloe, K.; Jolliffe, K. A.; Lindoy, L. F.; Heine, A.; Doert, T.; Jager, A.; Gloe, K. *Polyhedron* **2011**, *30*, 708.
(54) Tamayo, A.; Lodeiro, C.; Escriche, L.; Casabo, J.; Covelo, B.; Gonzalez, P. *Inorg. Chem.* **2005**, *44*, 8105.
(55) Nolan, E. M.; Lippard, S. J. *J. Am. Chem. Soc.* **2003**, *125*, 14270 (Hg fluoroscein turn-on sensor).
(56) Yoon, S.; Albers, A. E.; Wong, A. P.; Chang, C. J. *J. Am. Chem. Soc.* **2005**, *127*, 16030.
(57) Caballero, A.; Martínez, R.; Lloveras, V.; Ratera, I.; Vidal-Gancedo, J.; Wurst, K.; Tárraga, A.; Molina, P.; Veciana, J. *J. Am. Chem. Soc.* **2005**, *127*, 15666.
(58) Aragoni, M. C.; Arca, M.; Bencini, A.; Blake, A. J.; Caltagirone, C.; De Filippo, G.; Devillanova, F. A.; Garau, A.; Gelbrich, T.; Hursthouse, M. B.; Isaia, F.; Lippolis, V.; Mameli, M.; Mariani, P.; Valtancoli, B.; Wilson, C. *Inorg. Chem.* **2007**, *46*, 4548.
(59) Lu, H.; Zhang, S. S.; Liu, H. Z.; Wang, Y. W.; Shen, Z.; Liu, C. G.; You, X. Z. *J. Phys. Chem. A* **2009**, *113*, 14081.